Reductions in Parachute Drag Due to Forebody Wake Effects

Carl W. Peterson* and Donald W. Johnson†
Sandia National Laboratories, Albuquerque, New Mexico

The drag of a 20-deg conical ribbon parachute was measured at several axial stations behind an ogive-cylinder forebody with and without fins. The same parachute was tested in "undisturbed" flow (where wake effects were negligible) so that the effects of suspension line length on parachute drag could be separated from the drag losses caused by the turbulent wake. Total head pressure surveys made across the forebody wake confirmed the validity of the assumption that the ratio of parachute drag behind a forebody divided by wake-free parachute drag is equal to the ratio of effective dynamic pressure acting on the parachute divided by freestream dynamic pressure. However, the inability of existing turbulent wake theoretical models to make accurate predictions of wake velocity distributions for arbitrary forebody shapes is a fundamental limitation of the drag loss analysis. If wake velocity profiles are known, the empirical constants in the turbulent wake theoretical models can be adjusted and accurate estimates of wake-induced parachute drag loss can be obtained from existing theory.

Nomenclature

a = see Eq. (7c)
b = turbulent wake width
C_1 = see Eq. (2)
C_2 = see Eq. (3)
C_A = parachute axial force coefficient
C_D = forebody axial force coefficient
C_N = forebody normal force coefficient
C_S = forebody streamwise force coefficient, $C_A \cos\alpha_B + C_N \sin\alpha_B$
D_1 = see Eq. (11a)
D_2 = see Eq. (11b)
D_B = forebody diameter
D_C = constructed parachute diameter
D_P = diameter of skirt of inflated canopy
H = constant relating apparent kinematic viscosity to momentum defect in turbulent wakes
k = see Eq. (7d)
L = suspension line length
m = see Eq. (7a)
n = see Eq. (7b)
P_s = freestream static pressure
P_t = total head pressure
q = dynamic pressure $= P_t - P_s = \frac{1}{2}\rho U^2$
q_{eff} = average effective dynamic pressure acting on the parachute
R = radial distance from forebody or wake centerline
R_B = body radius $= D_B/2$
R_P = $D_P/2$
r = R/R_B
r_P = R_P/R_B
S_B = cross-sectional area of forebody $= \pi R_B^2$
U = streamwise velocity
u = wake velocity defect $= U_\infty - U$
X = lateral position in wind tunnel; $X=0$ plane passes through center of model
Y = vertical position in wind tunnel; $Y=0$ plane passes through center of model
Z = streamwise distance downstream of forebody base
α_B = forebody angle of attack
α_{SL} = half-angle of suspension lines
ρ = density

Subscripts

B = pertaining to the forebody
CL = positioned on wake centerline
∞ = pertaining to freestream or wake-free conditions

Received Oct. 14, 1981; presented as Paper 81-1939 at the AIAA 7th Aerodynamic Decelerator and Balloon Technology Conference, San Diego, Calif., Oct. 21-23, 1981; revision received March 22, 1982.

*Supervisor, Parachute Systems Division. Associate Fellow AIAA.
†Member, Technical Staff, Parachute Systems Division. Associate Fellow AIAA.

Introduction

THE turbulent wake behind a forebody is characterized by reductions in streamwise velocity and dynamic pressure relative to the freestream (undisturbed) airflow. The low momentum air in the wake flows into the parachute canopy and, depending upon the drag of the forebody and the size of the canopy relative to the wake diameter, the resulting parachute drag loss due to the oncoming wake may be significant. Figure 1 shows the wake approaching the canopy and suggests the physical mechanism for the reduction in parachute drag.

Previous investigators have recognized the need to provide the parachute designer with a way to quantify the reduction in drag caused by the turbulent wake behind the forebody. An analytical model has been proposed, but the complexity of the wake/parachute interaction and the lack of a closed-form solution for turbulent wakes has made it necessary to impose several restrictive assumptions on the analytical model. An additional problem is the scarcity of experimental data which can be used to evaluate the simplified analytical model of wake-induced parachute drag reduction. The details of the analysis and a review of existing experimental data are summarized in the next section of this article.

The primary purpose of this present study is to obtain additional data for checking the drag reduction analysis and the physical model upon which the analysis is based. Specific objectives of this research are:

1) To measure parachute drag, both with and without wake effects, at known locations behind the forebody and to compare the measured wake-induced drag loss with predictions of the theory.

2) To survey the wake behind several forebody shapes, including realistic shapes with fins, and to compare measured velocity profiles and wake widths with the simplified theory (these results will expand the data base for evaluating empirical turbulent wake constants as a function of forebody shape and drag coefficient).

3) To measure the effective dynamic pressure acting on the parachute by integrating the measured dynamic pressure profiles across the canopy (these results will act as a check on the underlying physical assumption that the reduction in effective parachute drag is proportional to the difference between freestream and effective dynamic pressure).

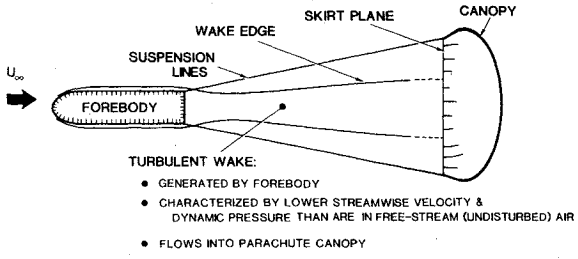

Fig. 1 Description of the interaction between the parachute and the forebody wake.

4) To provide data to evaluate the analysis at moderate forebody angles of attack.

Wake-Induced Parachute Drag Loss Analysis

Any analysis for predicting the wake-induced parachute drag loss must contain a model of the turbulent wake velocity distribution and a method of predicting how that velocity distribution affects the performance of the parachute. Both of these tasks involve complex and, in the case of turbulence, unsolved problems in fluid mechanics. There are no completely analytical descriptions of the turbulent wake for which simplifying assumptions have not been made. However, several approximate, semiempirical formulations[1-5] have been developed for the incompressible, turbulent, axisymmetric wake with no axial or radial static pressure gradients. In order to get a closed-form solution for a turbulent wake velocity distribution, it is assumed that the velocity defect on the wake centerline (u_{CL}) is small compared to the freestream velocity (U_∞); this assumption is only valid many forebody diameters downstream of the forebody base. Similarity solutions are postulated for the wake width $b(Z)$, the radial coordinate R, and $u_{CL}(Z)$. Assumptions about turbulent mixing lengths and turbulent shear stresses are also made. The resulting linearized equation for the streamwise velocity defect distribution in the turbulent wake is presented below in the form used by Heinrich and Riabokin[4]:

$$\frac{u}{U_\infty} = C_1 \exp\left[C_2 r^2\right] \tag{1}$$

where

$$C_1 = \frac{0.097}{(Z/D_B)^{2/3}} \left[\frac{C_D}{H^2}\right]^{1/3} \tag{2}$$

$$C_2 = \frac{-0.193}{(C_D HZ/D_B)^{2/3}} \tag{3}$$

and

$$r = R/R_B \tag{4}$$

The parameter H is an empirical constant used in the calculation of the turbulent apparent kinematic viscosity. It is defined using experimental values of the velocity defect on the centerline of the wake. Setting $r=0$ in Eq. (1) and using Eq. (2) gives

$$H = \frac{0.0302\sqrt{C_D}}{(Z/D_B)(u_{CL}/U_\infty)^{3/2}} \tag{5}$$

Heinrich and Eckstrom[5] have proposed a more general formulation of the velocity distribution in the turbulent wake in an attempt to obtain better agreement with experimental results closer to the forebody, where small drogue parachutes will probably be located. This formulation introduces four empirical constants (a, k, m, and n) for determining similarity expressions for defect velocity, wake width, and radial coordinate. The velocity distribution expression given in Ref. 5 is

$$\frac{u}{U_\infty} = \frac{a}{(Z/D_B)^m} \exp\left[\frac{-r^2}{0.435k^2(Z/D_B)^{2n}}\right] \tag{6}$$

Values of the four empirical constants were obtained in Ref. 5 for a wide variety of forebody shapes, including an ogive-cylinder similar to the one used in this experiment. By matching Eq. (6) to the experimental values of u/U_∞ on the wake centerline and at an arbitrary wake boundary location, the empirical constants were found to be

$$m = 0.85 \tag{7a}$$

$$n = 0.47 \tag{7b}$$

$$a = 0.42\exp(0.99C_D) \tag{7c}$$

$$k = 0.54\exp(0.84C_D) \tag{7d}$$

The corresponding equation for H is

$$H = \frac{nk(Z/D_B)^{m+n-1}}{9.20a} \tag{8}$$

Predictions from both wake models [Eqs. (1-5) and Eqs. (6-8)] will be evaluated against wake survey data from this experiment.

A first step toward the application of incompressible turbulent wake similarity theory to predictions of wake-induced parachute drag loss was taken by Heinrich and Riabokin.[4] Although they did not derive any method for predicting the drag loss, these investigators recognized that the drag loss is directly related to the reduction of dynamic pressure in the turbulent wake. The 1963 Parachute Handbook[6] derived an equation for the drag loss in terms of the ratio of the dynamic pressure on the wake centerline divided by the freestream dynamic pressure. The resulting expression predicted that reductions in parachute drag are larger close to the forebody than far downstream from it, but that equation was unable to predict the effects of parachute diameter on drag loss. Etherton et al.[7] realized that the drag loss is determined by reductions in wake dynamic pressure across all of the wake intercepted by the canopy, not just on the wake centerline. These investigators integrated the equation for the wake dynamic pressure distribution over the area of the inflated canopy skirt to get the effective average value of dynamic pressure acting on the parachute. The ratio of this effective dynamic pressure to the freestream dynamic pressure was equated to the ratio of actual parachute drag (with wake-induced drag losses) to ideal parachute drag (with no forebody wake effects). The resulting equation for parachute drag loss ratio, which was reproduced erroneously in Refs. 7 and 8, is obtained by integrating the dynamic pressure ratio q/q_∞ from the wake centerline to the skirt radius of the inflated parachute:

$$\frac{C_A}{C_{A\infty}} = \frac{q_{\text{eff}}}{q_\infty} = \frac{1}{\pi R_P^2}\int_0^{R_P}\left(1-\frac{u}{U_\infty}\right)^2 2\pi R\,dR$$

$$= 1 + \frac{2}{r_P^2}\cdot\frac{C_1}{C_2}\cdot\left[1 - e^{C_2 r_P^2} + \frac{C_1}{4}e^{2C_2 r_P^2} - \frac{C_1}{4}\right] \tag{9}$$

If Eqs. (6-8) are used instead of Eqs. (1-5) in the derivation of parachute drag loss ratio, Eq. (9) is replaced by

$$\frac{C_A}{C_{A\infty}} = 1 + \frac{2}{r_P^2}\cdot\frac{D_1}{D_2}\cdot\left[1 - e^{D_2 r_P^2} + \frac{D_1}{4}e^{2D_2 r_P^2} - \frac{D_1}{4}\right] \tag{10}$$

where

$$D_1 = \frac{a}{(Z/D_B)^m} \tag{11a}$$

and

$$D_2 = \frac{-1.0}{0.435k^2(Z/D_B)^{2n}} \tag{11b}$$

Experimental data are available which validate the analytical description of velocity profiles in the turbulent wakes behind a limited number of slender and bluff forebodies.[4,5,9] However, there is very little experimental data which can be used to evaluate the analytical method for predicting wake-induced parachute drag reduction. Experiments by Heinrich and Haak,[10] wherein the drag of flat plates, cones, and hemispheres was measured in the turbulent wake of a forebody, are the only existing measurements of wake-induced drag reduction known to the authors in the open literature.

Description of the Experiment

The forebody model used for this experiment is shown in Fig. 2. The model is basically an ogive-cylinder which could be configured with no fins, three fins (in the inverted "Y" position), or four fins (in "plus" and "X" positions) on the aft body section. It is 114 mm (4.5 in.) in diameter and 916 mm (36 in.) long. Parachute drag and wake survey results were obtained for each fin configuration. The model was mounted in the 7×10-ft Vought Corporation Low Speed Wind Tunnel test section using six steel cables 4.76 mm (0.1875 in.) in diameter. By adjusting the cable length and anchor positions, the forebody angle of attack (α_B) could be set at 0, 10, and 20 deg. Figure 3 is a model installation sketch for $\alpha_B = 10$ deg.

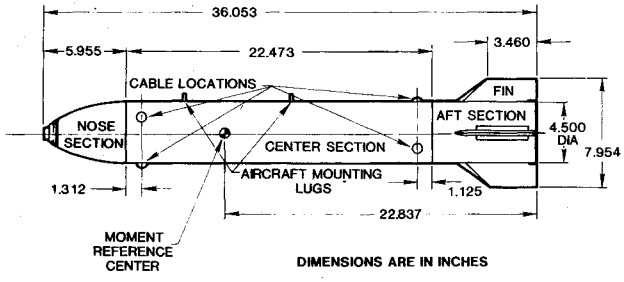

Fig. 2 Forebody model.

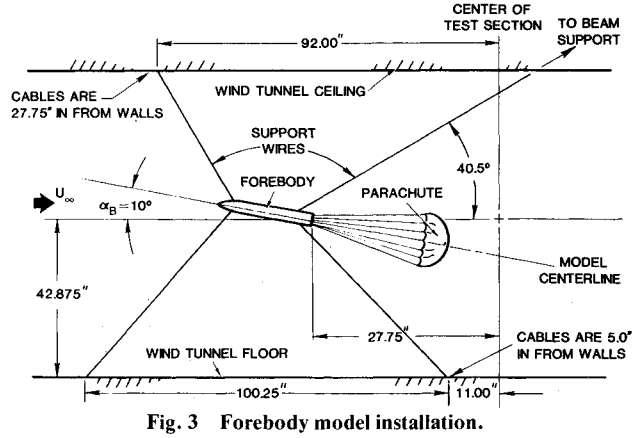

Fig. 3 Forebody model installation.

The parachute model, shown in Fig. 4, is a 20-deg conical ribbon nylon parachute with 12 gores and 10 ribbons. The canopy constructed diameter is 0.38 m (15 in.). Three miniradials extended from skirt to vent in each gore to stabilize the ribbons. The geometric porosity of this parachute, which is a quarter-scale model of an actual drogue parachute, is 19%. The suspension lines were fitted with loops so that the parachute canopy could be tethered at five different distances behind the forebody. The ratios of suspension line length (L) to constructed parachute diameter (D_C) used in the test were 1.00, 1.25, 1.50, 1.75, and 2.00. The loops were attached to an axial force balance located in the aft section of the model. Photographs of the parachute were taken at each α_B and L/D_C to measure the inflated canopy position, the angle of the suspension lines (α_{SL}), and the X and Y dimensions across the canopy skirt. This information was needed to determine the amount of forebody wake intercepted by the parachute.

Before installing the model for parachute drag and wake survey tests, the model was mounted on a force balance to obtain forebody drag and normal force coefficients (C_D, C_N) at each α_B for each fin configuration. These data are needed as inputs to the equations for calculating turbulent wake velocity distributions and parachute drag loss. For $\alpha_B = 0$ deg, values of C_D given in Table 1 were used directly in Eqs. (2), (3), (5), (7c), and (7d). For $\alpha_B = 10$ and 20 deg, the streamwise component (C_s) of C_D and C_N was used in place of C_D in these equations in an attempt to extend the analysis to moderate forebody angles of attack. All force coefficients are referenced to the forebody cross-sectional area (πR_B^2) and a base pressure equal to freestream static pressure.

Figure 5 shows the special experiment which was conducted to determine the drag of the parachute in the absence of the ogive-cylinder forebody for each suspension line length. Three 3.18-mm-diam (0.125-in.-diam) cables positioned a 44-mm-diam (1.74-in.-diam) cone-cylinder support body at the center of the tunnel. A small strain gage balance trailed behind the cone-cylinder on a 0.6-m (2-ft) cable. Another 0.6-

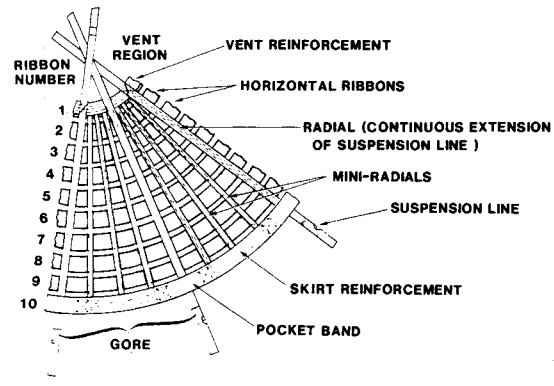

Fig. 4 20-deg conical ribbon parachute model.

Table 1 Forebody axial, normal, and streamwise force coefficients

Forebody configuration	$\alpha_B = 0$ deg			$\alpha_B = 10$ deg			$\alpha_B = 20$ deg		
	C_A	C_N	C_S	C_A	C_N	C_S	C_A	C_N	C_S
No fins	0.1321	...	...	0.1088	0.4556	0.1863	0.0371	1.2282	0.4549
X fins	0.1811	...	...	0.1371	0.9968	0.3081	0.0315	2.3917	0.8477
+ fins	0.1784	...	...	0.1358	1.1006	0.3249	0.0342	2.7390	0.9689
λ fins	0.1791	...	...	0.1383	0.9242	0.2967	0.0433	2.3710	0.8516

m cable and two swivels were attached to the downstream side of the balance. Fastened to the downstream side of the swivel was a small clevis, to which the parachute suspension lines were attached. The excess suspension line material at each L/D_C was cut off to prevent the excess suspension lines from becoming a "forebody" and generating a large wake in front of the canopy. The drag of the parachute in these tests was considered to be free from any significant wake effects because the forebody, balance, and wires were small and were located about 2 m (79 in.) upstream of the canopy. Photographs of inflated parachute skirt diameter and suspension line angle were made at each L/D_C.

An 80-tube total head pressure rake was used to survey the turbulent wake behind the model. The rake was mounted horizontally on a heavy support system which could be traversed vertically and axially behind the model while the tunnel was running. The middle of the rake was aligned with the center of the model. Axial survey positions were determined by the position of the parachute skirt for each L/D_C ratio. The rake was traversed vertically in the plane of the skirt (but without the parachute in the tunnel) from a Y location below the bottom edge of the parachute skirt in increments comparable to the 6.35-mm (0.25-in.) lateral spacing between total head tubes. At each Y location, the rake was held stationary while a Scanivalve and eight 17 kPa (2.5 lb/in.^{2}) differential transducers read the total head pressure (P_t) at all 80 tubes. Test section static pressure (P_s) was measured by a static probe near the wall on the tunnel vertical centerline. P_s was assumed to be constant across the test section and across the wake. This assumption is consistent with the assumptions in the analysis and is generally valid everywhere except in the near wake directly behind the forebody.

All wake surveys and parachute drag measurements (with and without the forebody) were made at a nominal freestream dynamic pressure (q_∞) of 4.8 kPa (100 lb/ft^2) and a nominal Reynolds number of 5.3×10^6, based upon forebody length. The dynamic pressure (q) at each pressure tap was obtained by subtracting P_s from P_t and using Bernoulli's equation for incompressible flow:

$$q=P_t-P_s=\tfrac{1}{2}\rho U^2 \tag{12}$$

Local values of q were nondimensionalized by the freestream dynamic pressure, which was determined from total head surveys outside of the forebody wake. Nondimensional wake velocities were also obtained by applying Bernoulli's equation:

$$U/U_\infty=\sqrt{q/q_\infty} \tag{13}$$

In regions of the wake where P_t was smaller than P_s, Bernoulli's equation is not valid and the streamwise velocity was assumed to be zero.

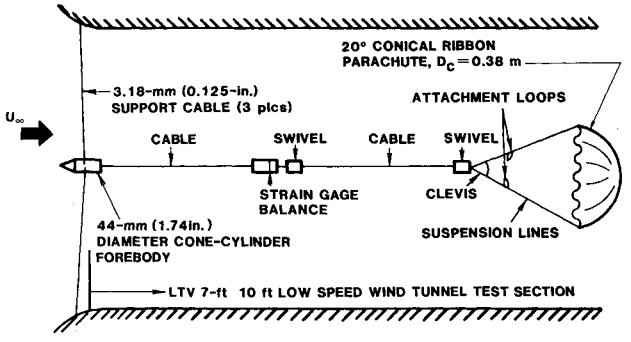

Fig. 5 Measurement of "wake-free" parachute drag.

Velocity Profiles in the Forebody Wake

Measured velocity distributions behind each forebody at $\alpha_B=0$ deg were compared to predictions by Heinrich and Riabokin[4] and Heinrich and Eckstrom.[5] Figure 6 presents these theoretical predictions and survey data behind the X-fin configuration at $Z/D_B=4.83$. The velocity distribution predicted by Heinrich and Riabokin was forced to match experimental data of u_{CL}/U_∞; values of H were determined as a function of Z/D_B for all forebody configurations at $\alpha_B=0$ deg. Good agreement between experimental and predicted values of u_{CL}/U_∞ were obtained for

$$H=0.02048-0.0002693\,(Z/D_B) \tag{14}$$

These values of H are considerably lower than those reported in Ref. 4. Furthermore, Fig. 6 shows that the theoretical Gaussian velocity distribution from Ref. 4 decays more rapidly with increasing values of r than the experimental distribution. The momentum defect in the wake is underpredicted by Eqs. (1-5). The empirical velocity distribution proposed by Heinrich and Eckstrom did not agree with the experimental distribution anywhere across the wake when their empirical expressions for a, k, m, and n [Eqs. (7a-7d)] were used with Eq. (6). The wake momentum defect is also underpredicted by these equations.

The poor agreement between present experimental velocity distribution data and both theoretical predictions points out a major weakness in the parachute drag loss analysis. The simplified turbulent wake velocity distribution equations, upon which the drag loss analysis is based, do not provide good predictions of velocity across the wake for any arbitrary forebody shape. However, if wake measurements are available, good agreement can be obtained by using Eq. (6) and fitting the empirical constants a, k, m, and n to the data. Using $\alpha_B=0$ deg data for the no-fin, X-fin, and inverted Y-fin bodies, the following expressions for the four constants were found to apply to the forebody configurations tested in this experiment:

$$m=0.64 \tag{15a}$$

$$n=0.33 \tag{15b}$$

$$a=0.51\cdot\exp(2.02C_D) \tag{15c}$$

$$k=0.85\cdot\exp(0.65C_D) \tag{15d}$$

The good agreement between present experimental velocity distribution data and the theory of Ref. 5 with modified constants [Eqs. (6) and (15)] for each forebody at $\alpha_B=0$ deg is typified in Fig. 7.

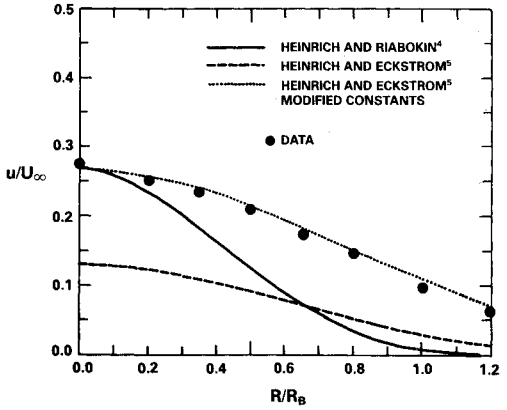

Fig. 6 Velocity distribution across the turbulent wake, $Z/D_B=4.83$, X-fin forebody, $\alpha_B=0$ deg.

Computer plots of three-dimensional wake velocity distribution data were generated so that the predominate flow features could be identified. A typical plot is shown in Fig. 8 for the X-fin configuration at $\alpha_B = 0$ deg. In addition to the forebody/fin wake, the wakes behind the six forebody support wires are very evident. Unfortunately, the parachute canopy intercepted portions of the wire wakes in addition to the forebody wake. The effect of the wire wakes on parachute drag was determined by replacing the wire wake velocity distribution by the freestream velocity and integrating the corrected velocity field across the canopy skirt to get a corrected effective dynamic pressure acting on the parachute. The corrected (no wire wake) value of q_{eff} was compared to the uncorrected (with wire wake) value of q_{eff}. The comparison showed that the wire wake reduced the effective dynamic pressure on the parachute by less than 1%, but the corrected survey data were used to provide a fair comparison with theory. The same small correction was applied to each parachute drag measurement obtained behind the forebody.

Additional wake survey velocity plots behind the no-fin and X-fin configurations at $\alpha_B = 0$ and 20 deg are presented in Figs. 9-13. The wakes behind the fins are swallowed by the forebody wake behind $Z/D_B = 3$ when the forebody is aligned with the freestream velocity. However, the fins dominate the wake structure when the forebody is pitched to $\alpha_B = 20$ deg. Trailing vortices from the fins appear as four "spikes" in Fig. 11, and the fin downwash changes the velocity distribution in the forebody wake. Without fins, the forebody wake at $\alpha_B = 20$ deg is similar in shape to the wake at $\alpha_B = 0$ deg, but it has a larger momentum defect and is displaced toward negative Y values by the downwash from the forebody. The major differences in wake structure caused by the fins have a

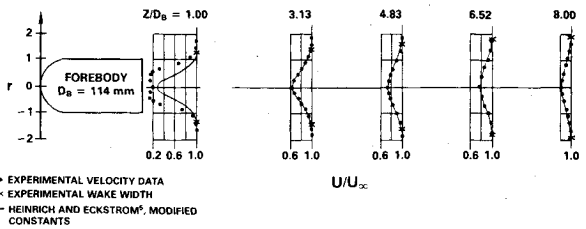

Fig. 7 Experimental and theoretical velocity distributions behind X-fin forebody.

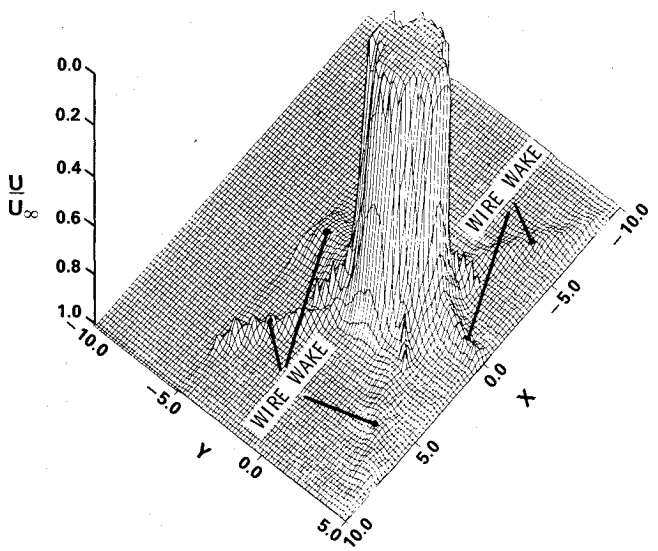

Fig. 8 Measured wake velocity profiles, X-fin forebody configuration, $\alpha_B = 0$ deg, $Z/D_B = 0.50$.

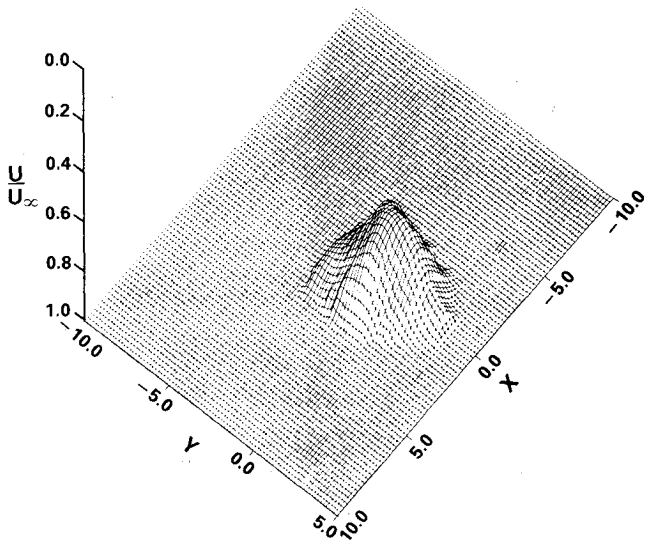

Fig. 10 Measured wake velocity profiles, X-fin forebody configuration, $\alpha_B = 0$ deg, $Z/D_B = 3.10$.

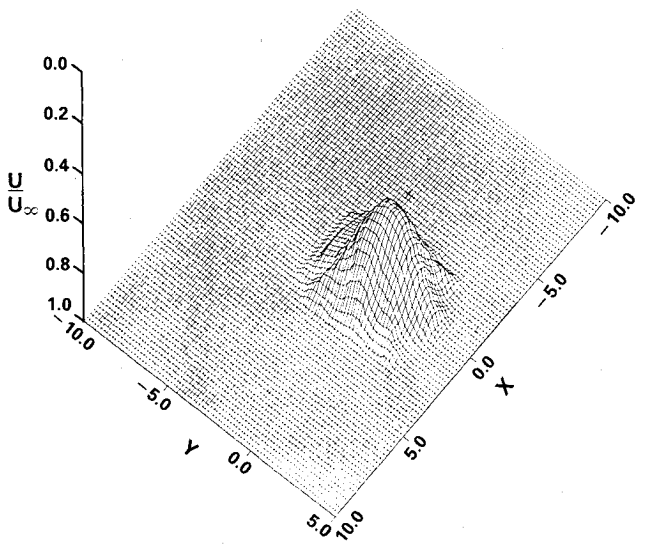

Fig. 9 Measured wake velocity profiles, X-fin forebody configuration, $\alpha_B = 0$ deg, $Z/D_B = 3.13$.

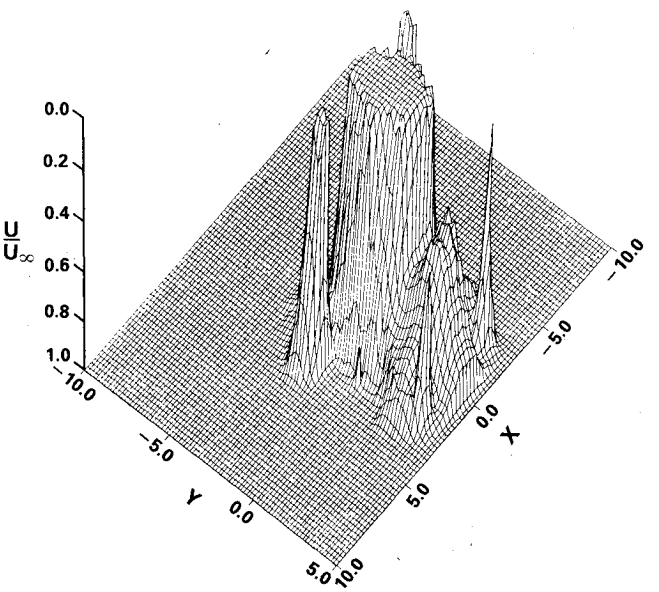

Fig. 11 Measured wake velocity profiles, X-fin forebody configuration, $\alpha_B = 20$ deg, $Z/D_B = 0.50$.

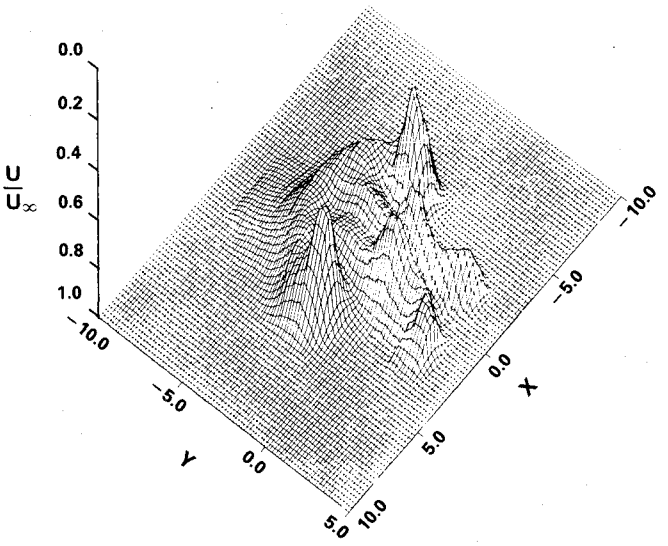

Fig. 12 Measured wake velocity profiles, X-fin forebody configuration, $\alpha_B = 20$ deg, $Z/D_B = 3.39$.

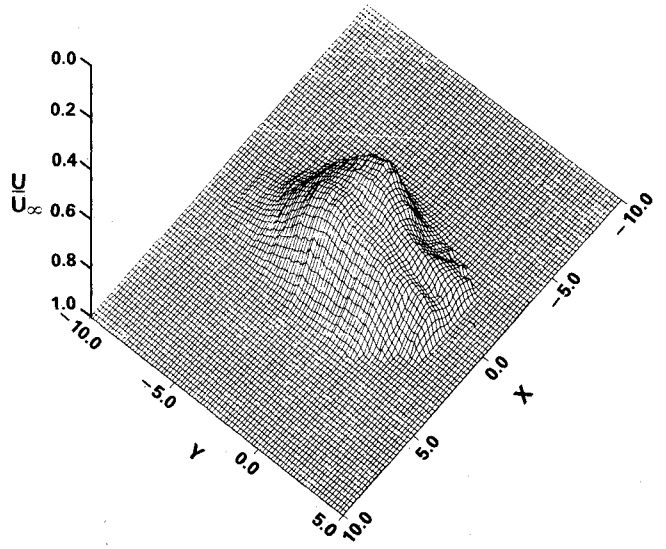

Fig. 13 Measured wake velocity profiles, no-fins forebody configuration, $\alpha_B = 20$ deg, $Z/D_B = 3.40$.

significant effect upon the ability of the simplified wake-induced drag loss analysis to predict accurately the reduction in parachute drag at forebody angles of attack, as will be shown in a later section of this article.

Measurements of Parachute Drag

The wake-free parachute drag measurements, plotted in Fig. 14, show the strong effect of suspension line angle on parachute axial force coefficient. As suspension line angle increases, the inward radial component of suspension line load becomes larger and causes the canopy to assume a smaller diameter and more streamlined shape. These changes cause corresponding decreases in $C_{A\infty}$. The wake-free drag data were correlated to α_{SL} by a linear least-squares curve fit:

$$C_{A\infty} = 0.7631 - 0.01311\alpha_{SL} \tag{16}$$

The correct value of $C_{A\infty}$ for nondimensionalization of parachute axial force coefficients measured behind the forebody (C_A) is the value obtained at the same suspension line angle as was observed when the parachute was in the forebody wake. Unless values of C_A and $C_{A\infty}$ are taken at the same suspension line angle, the differences in drag due to

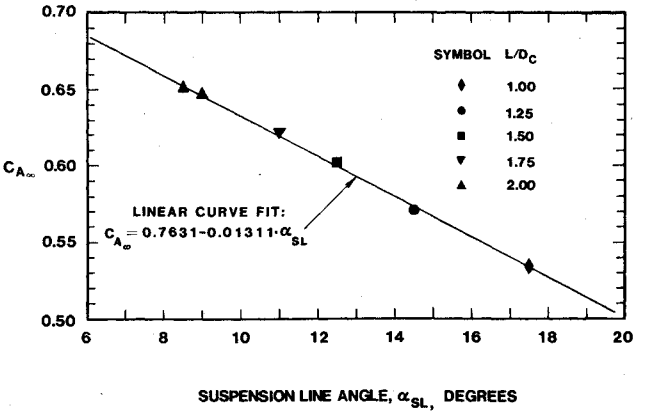

Fig. 14 Wake-free parachute drag measurements.

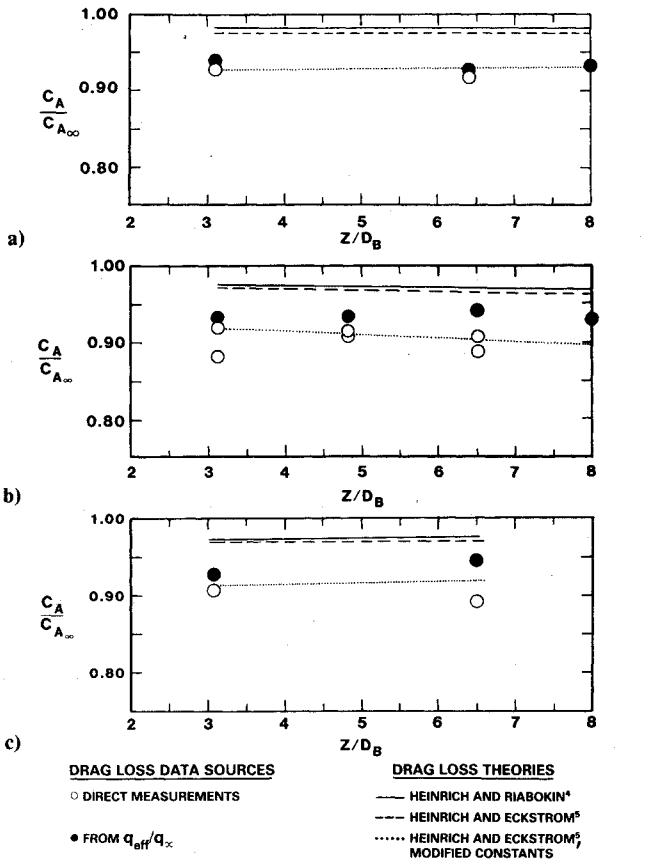

Fig. 15a) Comparison of drag loss data with theory, $\alpha_B = 0$ deg, no-fin forebody configuration. b) Comparison of drag loss data with theory, $\alpha_B = 0$ deg, X-fin forebody configuration. c) Comparison of drag loss data with theory, $\alpha_B = 0$ deg, inverted Y-fin forebody configuration.

canopy size and shape will obscure the differences in drag due to forebody wake effects.

Measured values of parachute drag loss ratio $C_A/C_{A\infty}$ are compared with measurements of q_{eff}/q_∞ from wake surveys in Fig. 15 for three forebody configurations at $\alpha_B = 0$ deg. Good agreement was observed between measured values of $C_A/C_{A\infty}$ and those derived by integrating the measured dynamic pressure distribution across the canopy skirt and assuming

$$C_A/C_{A\infty} = q_{\text{eff}}/q_\infty \tag{17}$$

Equation (17) is a statement of the fundamental physical model of parachute/wake interaction underlying the

analytical predictions of parachute wake-induced drag loss. The present experimental data for $\alpha_B = 0$ deg validate that physical model.

Theoretical drag loss calculations for $\alpha_B = 0$ deg are also compared to experimental results on Fig. 15. In these and all subsequent figures, the theory labeled "Heinrich and Riabokin" refers to the velocity distribution theory of Ref. 4 [Eqs. (1-5)] and the corresponding drag loss formulation [Eq. (9)]. The theory labeled "Heinrich and Eckstrom" refers to the velocity profile equations from Ref. 5 [Eqs. (6) and (8)], the empirical wake constants from the same reference [Eqs. (7a-7d)], and the drag loss formulation given by Eqs. (10) and (11). Both of these drag loss theories predict smaller reductions in parachute drag than were measured in this experiment. This result is not surprising in view of the fact that both velocity distribution theories underestimate the momentum defect in the wake.

The "modified Heinrich and Eckstrom" drag loss theory shown on Fig. 15 uses Eqs. (6) and (8) for calculating velocity profiles, but uses the empirical expressions for *a, k, m,* and *n* determined from present wake velocity profile data [Eqs. (15a-15d)] instead of the expressions derived in Ref. 5. Equations (10) and (11) are used to calculate drag loss. This modified theory shows good agreement with experimental drag loss data at $\alpha_B = 0$ deg because the empirical wake constants were adjusted to match the wake velocity distributions. The success of the modified theory reinforces the validity of Eq. (17), but it also indicates that good predictions of parachute drag loss can be expected only if an accurate method of calculating turbulent wake velocity profiles is available.

Comparisons of drag loss data with theory and effective dynamic pressure ratio (q_{eff}/q_∞) are shown for the same forebody configurations at $\alpha_B = 10$ deg in Fig. 16. In each case, measured values of drag loss ratio agree with the effective dynamic pressure ratio to within 3%. The Heinrich and Riabokin and Heinrich and Eckstrom theories predict higher values of $C_A/C_{A\infty}$ than were measured, as they did for $\alpha_B = 0$ deg. The theory of Heinrich and Eckstrom with modified constants predicted values of parachute drag loss for the no-fin forebody configuration with the same accuracy that was achieved at $\alpha_B = 0$ deg. For the two-finned configurations, however, the modified theory predicted lower values of $C_A/C_{A\infty}$ than were observed.

Figure 17 shows that agreement between measured values of $C_A/C_{A\infty}$ at $\alpha_B = 20$ deg and those derived from wake survey dynamic pressures was not as good as it was at lower forebody angles of attack. Furthermore, none of the theoretical predictions are applicable at $\alpha_B = 20$ deg, even when C_s is used in place of C_D. Correlations with C_s become inaccurate when the forebody angle of attack is large enough to make $C_A \cos \alpha_B \cong C_N \sin \alpha_B$. For the no-fin forebody, the maximum forebody angle of attack to which the theory can be extended was approximately 10 deg. For the finned forebodies, the maximum α_B was lower.

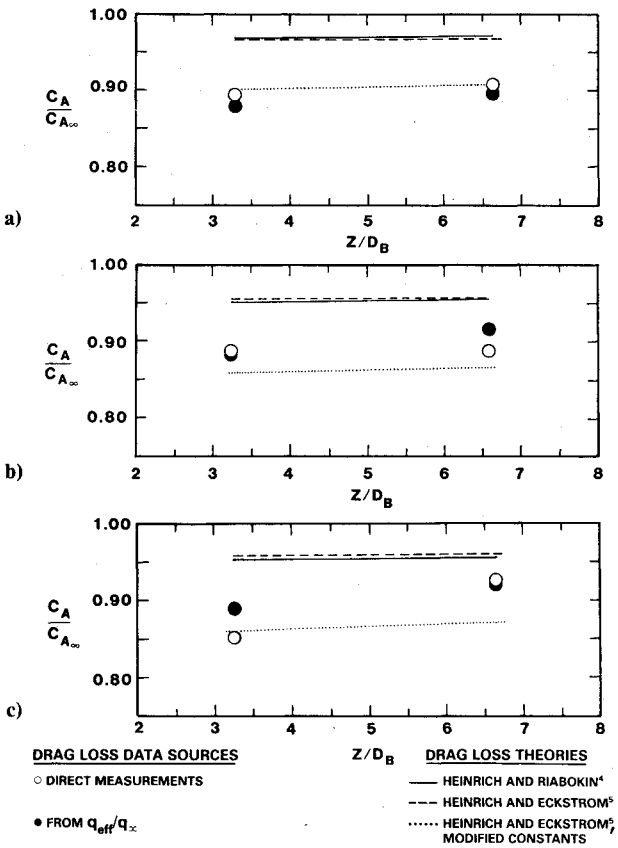

Fig. 16a) Comparison of drag loss data with theory, $\alpha_B = 10$ deg, no-fin forebody configuration. b) Comparison of drag loss data with theory, $\alpha_B = 10$ deg, X-fin forebody configuration. c) Comparison of drag loss data with theory, $\alpha_B = 10$ deg, inverted Y-fin forebody configuration.

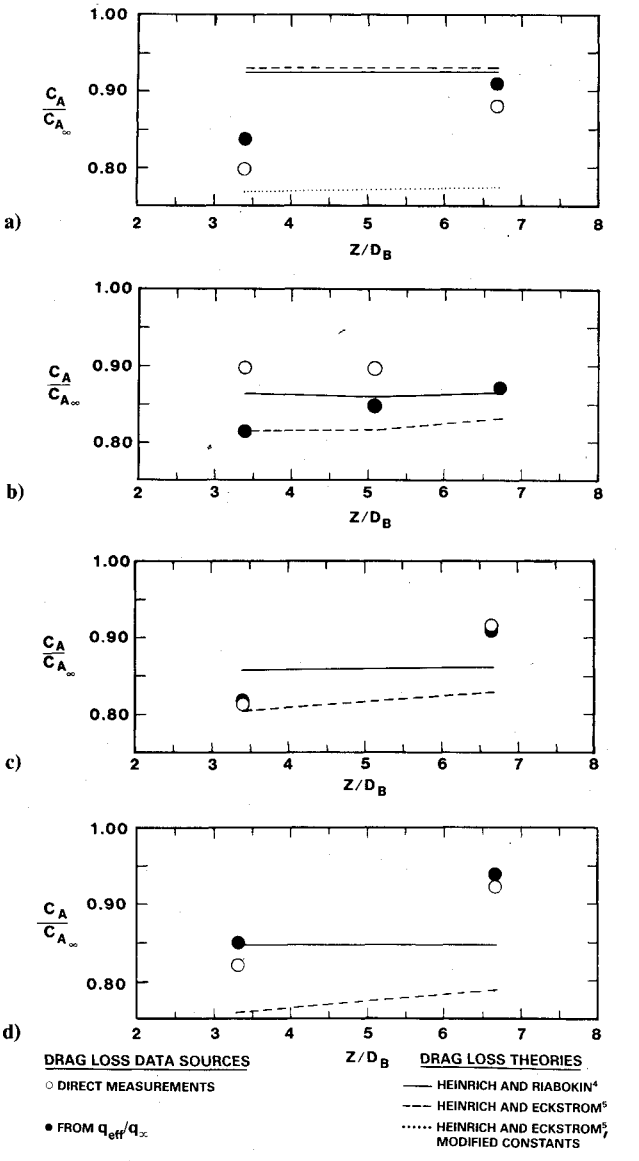

Fig. 17a) Comparison of drag loss data with theory, $\alpha_B = 20$ deg, no-fin forebody configuration. b) Comparison of drag loss data with theory, $\alpha_B = 20$ deg, X-fin forebody configuration. c) Comparison of drag loss data with theory, $\alpha_B = 20$ deg, inverted Y-fin forebody configuration. d) Comparison of drag loss data with theory, $\alpha_B = 20$ deg, plus-fin forebody configuration.

Conclusions

An experiment was conducted to evaluate approximate analytical methods for predicting the reduction in parachute drag due to forebody wake effects. Velocity distributions were measured behind realistic forebody configurations and compared to three different turbulent wake velocity models. These velocities were integrated to determine the average effective dynamic pressure acting on the parachute. Comparisons among drag loss data, effective dynamic pressure ratios, and theoretical predictions were made for no-fin and finned forebodies at angles of attack of 0, 10, and 20 deg. The major conclusions drawn from these comparisons are summarized below.

1) The ratio of measured parachute drag behind a forebody divided by the wake-free parachute drag was found to be equal to the ratio of the average dynamic pressure acting on the parachute divided by the freestream dynamic pressure. This conclusion applied to each forebody at $\alpha_B = 0$, 10, and (with slightly reduced accuracy) 20 deg.

2) Two approximate analytical methods for predicting turbulent wake velocity distributions were found in the literature and their predictions were compared to wake velocity measurements behind three forebody configurations at $\alpha_B = 0$ deg. Both methods were unable to predict wake widths and total momentum defect correctly. As a result, the drag loss theories which use these turbulent wake velocity distribution methods predicted values of $C_A/C_{A\infty}$ which were higher than measured values. The inability of existing turbulent wake theoretical models to provide accurate predictions of wake velocity distributions for arbitrary forebody shapes is a fundamental limitation of the wake-induced parachute drag loss analysis.

3) Good agreement between wake velocity data and predictions by Heinrich and Eckstrom[5] can be obtained by modifying the expressions for the empirical turbulent wake constants. Predictions of $C_A/C_{A\infty}$ from the drag loss theory agreed well with present data at $\alpha_B = 0$ deg when the modified expressions for empirical wake constants were used instead of the expressions given in Ref. 5.

4) If empirical turbulent wake constants can be determined to give accurate predictions of parachute drag loss at $\alpha_B = 0$ deg, the same theory and constants should provide accurate drag loss predictions at moderate forebody angles of attack if the streamwise forebody force coefficient C_s is used in the theory in place of C_D. The maximum angle of attack for which accurate predictions can be expected depends upon the forebody geometry and lift.

Acknowledgments

This work was sponsored by the U.S. Department of Energy. The authors are also indebted to H.E. Widdows for building the model parachute, P.R. Schatzle and R.E. Tate for assistance in conducting wind tunnel tests, and R.J. Buffington, R.E. French, R. Palmer, and A.E. McIntyre for reducing and plotting wind tunnel data.

References

[1] Swain, L.M. "Turbulent Wake Behind a Body of Revolution," *Proceedings of the Royal Society of London, Series A*, Vol. 125, 1929.

[2] Schlichting, H., *Boundary Layer Theory*, 4th ed., McGraw Hill, New York, 1960, Chaps. XIX and XXIII.

[3] Goldstein, S., "On the Velocity and Temperature Distribution in the Turbulent Wake Behind a Heated Body of Revolution," *Proceedings of the Cambridge Philosophical Society*, Vol. 34, 1938.

[4] Heinrich, H.G. and Riabokin, T., "Analytical and Experimental Consideration of the Velocity Distribution in the Wake of a Body of Revolution," Wright Air Development Division Report WADD 60-257, Dec. 1959.

[5] Heinrich, H.G. and Eckstrom, D.J., "Velocity Distribution in the Wake of Bodies of Revolution Based on Drag Coefficient," Air Force Flight Dynamics Laboratory Report ASD TDR-62-1103, Dec. 1963.

[6] Chernowitz, G. and DeWeese, J.H., "Performance of and Design Criteria for Deployable Aerodynamic Decelerators," Air Force Flight Dynamics Laboratory Report ASD-TR-61-579, Dec. 1963, pp. 204-219.

[7] Etherton, B.D., Burns, F.T., and Norman, L.C., "B58 Escape Capsule Stabilization Parachute System Development," General Dynamics Report FZA-4-408, Feb. 1962.

[8] Ewing, E.G., Bixby, H.W., and Knacke, T.W., "Recovery Systems Design Guide," Air Force Flight Dynamics Laboratory Report AFFDL-TR-78-151, Dec. 1978, pp. 277-293, 373-376.

[9] Hall, A.A. and Hislop, G.S., "Velocity and Temperature Distributions in the Turbulent Wake Behind a Heated Body of Revolution," *Proceedings of the Cambridge Philosophical Society*, Vol. 34, 1938.

[10] Heinrich, H.G. and Haak, E.L., "The Drag of Cones, Plates and Hemispheres in the Wake of a Forebody in Subsonic Flow," Air Force Flight Dynamics Laboratory Report ASD-TR-61-587, Dec. 1961.